Transitions between different channels in molecular nonsequential double ionization by few-cycle laser pulses

Qingbin Tang,[1,2] Cheng Huang,[1] Yueming Zhou,[1] Pengfei Lan,[1,*] and Peixiang Lu[1,†]

[1]*School of Physics and Key Laboratory of Fundamental Physical Quantities Measurement of Ministry of Education, Huazhong University of Science and Technology, Wuhan, 430074, China*

[2]*College of Physics and Electronic Engineering, Xinyang Normal University, Xinyang 464000 China*

(Received 22 January 2014; published 22 May 2014)

The carrier-envelope-phase (CEP) dependence of correlated electron dynamics in molecular nonsequential double ionization by few-cycle laser pulses is investigated with the three-dimensional classical ensemble model. Our results show that the asymmetric longitudinal momentum spectra of the doubly charged ions strongly depend on the CEP of the laser pulses, and the CEP-dependent asymmetry in the ions' momentum spectra varies with varying internuclear distance. By tracing the classical trajectories, it is found that the ionization dynamics of the first electron greatly affects the asymmetry. Back analysis reveals that with increasing internuclear distance, the pathway responsible for energy transfer between the two electrons changes from the recollision process to the collision process. This change causes the shape of the CEP-averaged ion momentum distribution to show a double-single-triple peak structure as the internuclear distance increases.

DOI: 10.1103/PhysRevA.89.053419 PACS number(s): 32.80.Rm, 32.80.Fb

I. INTRODUCTION

Nonsequential double ionization (NSDI) [1] is one of the most interesting phenomena in strong-field ionization as it involves the correlated motion of two electrons. Many experimental and theoretical studies [2–8] have addressed the underlying mechanisms for different target species, pulse durations, intensities, and wavelengths in the past three decades. Nowadays, the widely accepted picture of NSDI is the quasiclassical rescollision model [9]. According to this recollision scenario, an electron is ionized by the laser field. Then it is driven by the oscillating electric field and returns to the parent ion as the electric field reverses its direction, recolliding with the ion inelastically and leading to the release of the second electron in a direct recollision ionization process or indirectly via recollision-induced excitation with subsequent field ionization (RESI) [3].

With the rapid advance of ultrafast laser technology, intense ultrashort laser pulses with durations as short as a very few optical cycles have been generated and become available tools [10]. Since the electronic motions in atoms and molecules, which are on the attosecond scale, can directly respond to the instantaneous field of the driving pulse, the carrier-envelope phase (CEP) or absolute phase of the few-cycle pulses dramatically influences the ultrafast laser-matter interaction processes [11], such as high-harmonic generation [10], above-threshold ionization [12], laser-induced NSDI [13], and electron localization [14]. For NSDI, by controlling the CEP, few-cycle laser pulses can achieve only one single recollision event contribution to NSDI, which is of great importance for the understanding of correlated electron emissions. Previous experiments have measured the momentum distribution of doubly charged ions from NSDI by few-cycle laser pulses [13] and found strong CEP dependence of the NSDI process. The correlated electron momentum spectra obtained from NSDI by few-cycle laser pulses have been explored in various theoretical studies [15]. Recently, the measurement of correlated momentum distributions for NSDI in the single-cycle limit has been presented [16–18] for two laser intensity regimes. For relatively low intensity, a linelike distribution parallel to the main diagonal in the correlated momentum spectra is observed for argon NSDI. A classical analysis illustrates that the ionization time difference between the two electrons released from a doubly excited state is crucial for the emergence of the linelike distribution [16]. At a relatively high laser intensity, the measured two-electron correlated distributions arising from NSDI of argon [17] and nitrogen [18] all exhibit a cross-shaped structure that qualitatively differs from spectra recorded in all previous experiments using many-cycle pulses. With the help of classical trajectory diagnosis, the authors demonstrated that the RESI mechanism is responsible for the cross-shaped structure in the correlated momentum distribution.

Compared with the atomic case, the ionization dynamics of molecules is more complicated due to additional degrees of freedom [19]. For instance, the ionization probability of molecules changes with the internuclear distance, reaching a maximum at a critical distance [20]. Moreover, recent experiments have measured the angular distributions from NSDI [21] for stretched molecules, and found a strong internuclear-distance dependence of the NSDI process [22]. In this paper, the correlated electron dynamics in molecular NSDI driven by few-cycle pulses is investigated using the full three-dimensional (3D) classical ensemble model [23]. The results show that the asymmetric momentum spectra of doubly charged ions sensitively depend on the CEP and the internuclear distance. Back analysis reveals that the asymmetry of the ion momentum spectra is closely related to the ionization dynamics of the first electron. In particular, by tracing the classical trajectories, it is found that the responsible double-ionization (DI) pathway is transformed from the RESI channel to the collision-induced excitation with subsequent field ionization (CESI) channel with increasing internuclear distance. This transformation of NSDI channels leads to the

*Corresponding author: pengfeilan@hust.edu.cn

†Corresponding author: lupeixiang@mail.hust.edu.cn

 ©2014 American Physical Society

result that the shape of the CEP-averaged ion momentum distribution shows a double-single-triple peak structure as the internuclear distance increases.

This paper is organized as follows. In Sec. II we briefly describe the computation model. The results of the calculation are shown in Sec. III. The mechanisms for NSDI at different internuclear distances are presented and discussed in Sec. IV. In Sec. V the CEP effects on the ionization dynamics are analyzed. Finally, we summarize our results in Sec. VI.

II. THE CLASSICAL ENSEMBLE MODEL

The classical ensemble model proposed by Eberly and co-workers [23] has been widely used to study DI of atoms and molecules in intense laser fields [23,24]. In this study, we use this model to investigate the NSDI of diatomic molecules by few-cycle laser fields. The evolution of the system in this model is determined by the classical motion equation (atomic units are used throughout the paper if not stated otherwise) $d^2\mathbf{r}_i/dt^2 = -\mathbf{E}(t) - \nabla[V_{ne}(\mathbf{r}_i) + V_{ee}(\mathbf{r_1}, \mathbf{r_2})]$, where the subscript i labels the two different electrons and $\mathbf{E}(t)$ is a linearly polarized electric field. In the present calculations, the laser pulse is a few-cycle pulse with polarization direction along the z axis. Its electric field is $\mathbf{E}(t) = \hat{\mathbf{e}}_z E_0 \sin^2(\pi t/\tau)\cos(\omega t + \phi)$, where $\hat{\mathbf{e}}_z$ is the polarization vector. E_0, ω, T, ϕ, and τ are the amplitude, frequency, period, CEP, and the total duration of the pulse, respectively. The wavelength $\lambda = 780$ nm and the intensity $I = 1.5 \times 10^{14}$ W/cm^2. The total duration of the pulse contains four laser cycles, where the full width at half maximum (FWHM) is about 3.8 fs. The nucleus-electron and electron-electron interactions are represented by a 3D soft-core Coulomb potential $V_{ne} = -1/\sqrt{(\mathbf{r}_1 + R/2)^2 + a^2} - 1/\sqrt{(\mathbf{r}_1 - R/2)^2 + a^2} - 1/\sqrt{(\mathbf{r}_2 + R/2)^2 + a^2} - 1/\sqrt{(\mathbf{r}_2 - R/2)^2 + a^2}$ and $V_{ee} = 1/\sqrt{(\mathbf{r}_1 - \mathbf{r}_2)^2 + b^2}$, respectively. R is the internuclear distance which is aligned along the z axis. In this work, we vary the internuclear distance from 2 to 12 a.u. For each R, the ground-state energy of the model molecules is obtained from [25], corresponding to hydrogen molecules. In our calculations, the target is just a simple classical model for a diatomic molecule. When a molecule is exposed to strong laser fields, since the energy levels can be shifted by the electric field by an amount comparable to the field-free energy level differences, the discrete character of the energy spectrum of a molecule is weakened. Thus, a classical model molecule including an infinite number of excited states often behaves very well and reveals many detailed dynamics processes in strong-field ionization [24,26,27]. With the present laser intensity, due to the low collision energy, the two electrons are in bound states after collision and then released one by one by the laser field near the subsequent field maximum. This process of double ionization is not dependent on a particular excited state of an actual molecular system. In the equation presented above, a and b denote Coulomb softening parameters. As demonstrated in Ref. [24], the soft-core parameter a is employed to prevent autoionization, which sets the lower limit of a. There is also an upper limit for a, which is determined by the condition that there is a classically allowed region for the two electrons with the total energy of the ground-state energy of the target. For the targets investigated in this paper, the lower and upper limits of a are about 1.0 and 2.0 a.u., respectively. Here, as in Ref. [26], the parameter a is set to be 1.15 a.u. Note that a change of the parameter a has little impact on the statistical results presented in our paper. The parameter b is included to avoid a mathematical singularity in the calculations. Indeed the value of b has no physical meaning. It could be set to equal any other small value. In our work, we set $b = 0.05$ a.u.

In our calculation, the two nuclei of the model molecule are fixed at $(0,0,-R/2)$ and $(0,0,R/2)$, respectively. The initial state of the ensemble is obtained as follows. First, the two electrons are distributed around the two nuclei using a double-peak Gaussian probability distribution. Second, the available kinetic energy of the electron pairs is determined so that the system will have the energy of the ground-state energy (the sum of the first and the second ionization potentials of the model molecule). Any positions outside the classically allowed regions (which would give negative kinetic energy) are rejected. Third, the available kinetic energy is distributed between the two electrons randomly in momentum space. Finally and most importantly, the electrons are allowed to evolve for a sufficiently long time (200 a.u.) in the absence of the laser field to obtain stable position and momentum distributions [24]. When the initial state of the ensemble is obtained, the electric field is turned on and the entire process is determined by the classical motion equation presented above. After the laser pulse is turned off, we define double ionization if both electrons have positive energy.

III. CEP DEPENDENCE OF THE MOMENTUM SPECTRA FOR DIFFERENT INTERNUCLEAR DISTANCES

In Fig. 1, we present the longitudinal (parallel to the laser polarization direction, i.e., the z axis) momentum distributions of doubly charged ions for R from 2 to 12 a.u. The ion momenta are obtained as the sum of the momentum vectors of the two emitted electrons because the momentum of the absorbed photons is negligibly small [1]. The ion momentum spectra as a function of the CEP are plotted in the first and third columns. The second and fourth columns show the CEP-averaged ion momentum distributions for different internuclear distances. For all internuclear distances, the spectra exhibit a pronounced CEP-dependent asymmetry in the emission direction of the doubly charged ions (see the first and third columns in Fig. 1). When $R = 2$ a.u., the CEP-resolved ion momentum spectra [see Fig. 1(a)] are concentrated in a nonzero region and the CEP-averaged ion momentum distribution exhibits a clear double-hump structure [see Fig. 1(b)]. This is consistent with the recent experimental results on NSDI of nitrogen, where the shape of the CEP-averaged ion momentum distributions shows a pronounced double-hump structure [18]. With increase of the internuclear distances, Figs. 1(c), 1(e), and 1(g) show that the ion momentum spectra shift gradually to low momenta and the CEP-averaged ion momentum distributions evolve from a double-hump structure [see Fig. 1(b) and 1(d)] into a single-hump structure [see Fig. 1(h)]. As the internuclear distance increases further, instead, the ion momentum spectra shift to high momenta [see Figs. 1(i) and 1(k)]. When the

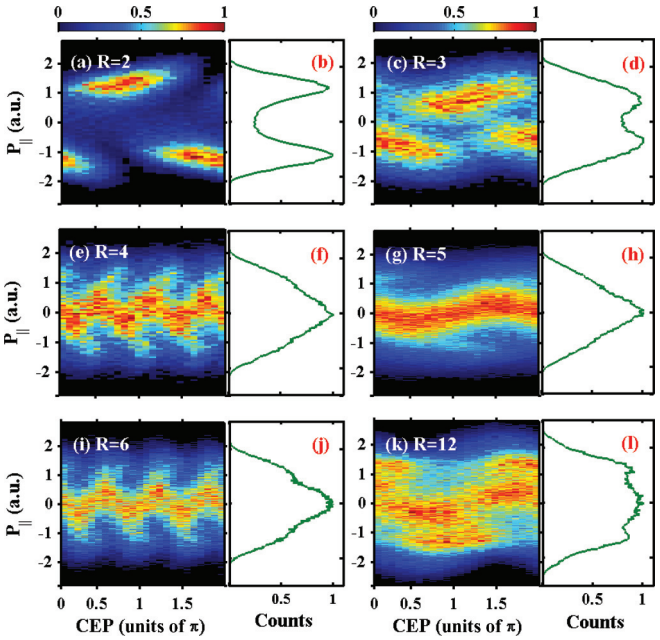

FIG. 1. (Color online) The CEP-resolved (the first and third columns) and CEP-averaged (the second and fourth columns) doubly-charged-ion longitudinal momentum distributions for NSDI by 780 nm linearly polarized few-cycle laser pulses. The laser intensity $I = 1.5 \times 10^{14}$ W/cm^2. The internuclear distance $R = 2$ a.u. (a),(b), 3 a.u. (c),(d), 4 a.u. (e),(f), 5 a.u. (g),(h), 6 a.u. (i),(j), and 12 a.u. (k),(l). For each CEP, the ensemble size is 3×10^6 in (a),(c), 0.5×10^6 in (e),(i), 1×10^6 in (g), and3×10^6 in (k).

internuclear distance increases to 12 a.u., as shown in Fig. 1(l), the CEP-averaged ion momentum distribution exhibits a triple-hump structure since a large part of the ion momentum spectra is concentrated in a nonzero region [see Fig. 1(k)]. These results indicate that for few-cycle pulses, the microscopic electron dynamics responsible for NSDI at various internuclear distances are different and complex.

In order to discuss the CEP dependence of the ion momentum spectra in more detail, we define an asymmetry parameter. The asymmetry parameter can be represented by the parameter $A = (N_- - N_+)/(N_- + N_+)$, where, for a given CEP ϕ, N_- and N_+ are the numbers of ions with a negative and positive momentum component along the polarization axis, respectively. The CEP-dependent asymmetry in doubly-charged-ion momentum spectra is displayed in Fig. 2. For each internuclear distance, the asymmetry parameter as a function of the CEP ϕ is shown in Fig. 2. The CEP-dependent asymmetry exhibits a sine-like behavior for different internuclear distances. Figure 2 shows that the amplitude of the asymmetry decreases rapidly at first and then increases slowly with increasing internuclear distances. Furthermore, the locations of the maximum (or minimum) values of the asymmetry curves are different at different internuclear distances. These results mean that the CEP-dependent asymmetry in the ion momentum spectra sensitively depends on the internuclear distance of the molecule, which may derive from the different dominant DI channels for different internuclear distances. Note that for each internuclear distance, although the ensemble size influences the smoothness of the asymmetry curves, the

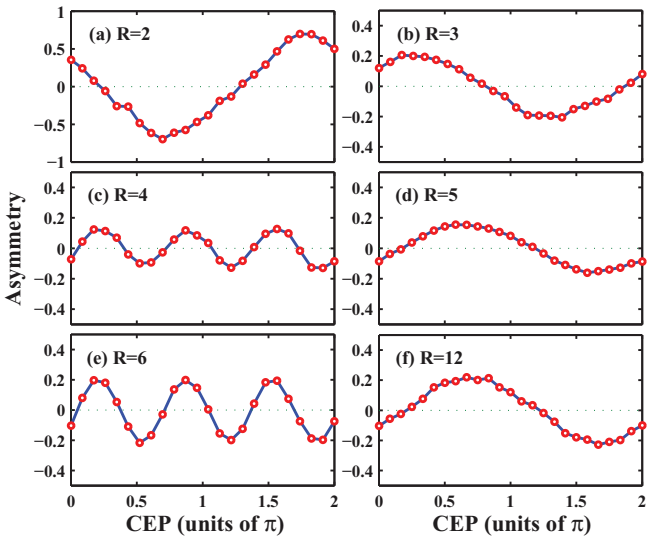

FIG. 2. (Color online) The asymmetries of the doubly-charged-ion momentum distributions as a function of CEP ϕ for different internuclear distances.

contributions of the various ionization channels to the total NSDI yields are almost unchanged.

IV. TRANSITIONS IN DIFFERENT CHANNELS OF ELECTRON EMISSION

Tracing back the temporal evolution of DI trajectories allows us to unveil the microscopic two-electron dynamics of strong-field molecular DI, and thus provides an intuitive way to identify the different ionization mechanisms. For each DI trajectory, the ionization time of the first electron t_{i1} is defined as the instant when the energy of one electron is above the suppressed barrier of the potential and with a velocity pointing to the outside direction of the potential well [24], where the energy of an electron includes kinetic energy, the ion-electron potential, and half of the electron-electron potential. The collision time t_c is defined to be the instant of closest approach after the first departure of one electron from the parent ion.

To explore the dynamical process responsible for the different structures of the doubly-charged-ion momentum spectra, we examine the delay time between t_c and t_{i1} for different internuclear distances. Figure 3 shows the counts of DI events versus delay time between t_c and t_{i1}. In Fig. 3 the delay times are plotted in units of optical cycle. For $R = 2$ a.u., the peak in Fig. 3(a) is located near $0.5T$ (where T is the length of the laser cycle), suggesting that most of the collisions occur near the zero crossing of the laser field. This is consistent with the prediction of the simple-man model [9]. Thus, the recollision process is the responsible dynamics for NSDI at small internuclear distances, while, with increase of the internuclear distance [see Figs. 3(a)–3(d)], the area under this peak becomes small, meaning that fewer DIs occur through the recollision process. For moderate and large internuclear distances, besides the peak located near $0.5T$, there is a peak near $0.125T$, and the area under this peak becomes large as the internuclear distance increases. Compared with the recollision

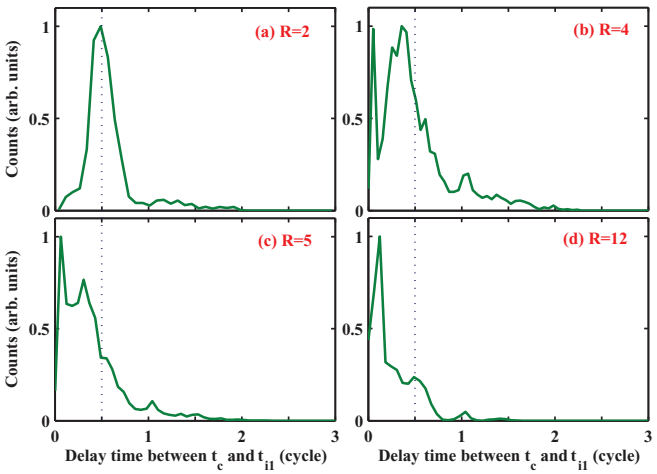

FIG. 3. (Color online) Counts of DI events versus delay time between collision time t_c and single-ionization time t_{i1}. $\phi = 0$ and the internuclear distances are 2 a.u. (a), 4 a.u. (b), 5 a.u. (c), and 12 a.u.(d).

process, the delay time is very short and the collision dynamics is defined as a direct collision process [27]. The different processes of NSDI in our calculations can be obtained by tracing the classical trajectories.

Two sample DI trajectories for the recollision mechanism (the left column) and the collision mechanism (the right column) are plotted separately in Fig. 4, presented as the longitudinal coordinate z (the upper row) and energy (the lower row) versus the emission time for each electron. For DI trajectories in the left column [see Figs. 4(a) and 4(b)], the energy transfer between the two electrons occurs through the well-known recollision process [9]. For DI trajectories in the right column [see Figs. 4(c) and 4(d)], the energy transfer occurs through a direct collision process where the first electron ionizes along the internuclear axis and transfers its energy to a second electron located near the neighboring

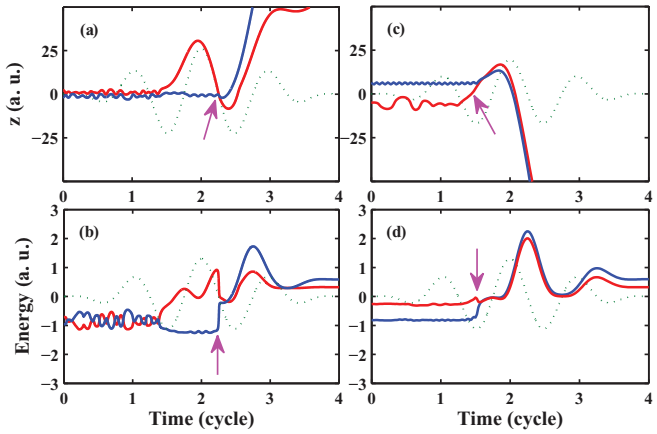

FIG. 4. (Color online) Two sample DI trajectories. The upper and lower rows show the longitudinal coordinate z (parallel to the laser polarization) and energy versus the time for emission of each electron, respectively. The arrows indicate the time when collision occurs. $\phi = 0$ and the internuclear distances are 2 a.u.(a),(b) and 12 a.u. (c),(d). The green dashed curve marks the laser electric field in arbitrary units.

nucleus. Through careful examination of the DI trajectories, we find that for the two collision processes, the most likely scenario for the laser intensity used in our work is the production of a doubly excited state (DES) [see Figs. 4(b) and 4(d)] after the collision. Because there is a subcycle delay time between DI and collision, the impact excitation DI channel is predominantly responsible for the DI process.

To give an overall understanding of the evolution of ion momentum distributions, we analyze the contributions of the different ionization channels to the total DI yield for different internuclear distances. Here, the NSDI trajectories are classified and segregated according to the delay time between the collision time and single-ionization time. This is a common and valid method of identification and analysis of electron dynamics in strong-field-ionization processes. As shown in Fig. 3, the statistical results show that for the RESI and CESI trajectories, the peaks of distributions of the delay time are located near $0.5T$ and $0.125T$, respectively. This means that the appropriate criterion is a value between $0.125T$ and $0.5T$. By analyzing large numbers of DI trajectories, it is found that a delay time of $0.2T$ is a suitable criterion for all internuclear distances. Thus, in our paper, the criterion of the delay time is set to be $0.2T$ for different internuclear distances. By back-tracing the trajectories, the DI pathway can be classified as the RESI channel if this time delay is larger than $0.20T$ and the CESI channel if it is less than $0.20T$.

We have also performed another analysis with different values of the criterion such as $0.15T$ and $0.25T$. The results show that the relative contributions of the RESI and CESI channels to the total DI yields are almost unchanged by a change of the criterion. For instance, for $R = 5$ a.u., when the values of the criterion are $0.15T$, $0.20T$, and $0.25T$, the contributions of the RESI channels to the DI are 39%, 38%, and 37%, respectively. When $R = 12$ a.u., the corresponding contributions of the CESI channels to the DI yields are about 72.8%, 74.1%, and 74.6%, respectively. These results indicate that the percentage contributions of the responsible ionization channels to the NSDI change very little when the values of the criterion change from $0.15T$ to $0.25T$.

As shown in Fig. 5, the relative contribution of different DI channels changes with the internuclear distance. Figure 5(a) shows that the contribution of the RESI channel to the total DI yield decreases quickly at first and then decreases slowly with increasing internuclear distance. Instead, as shown in

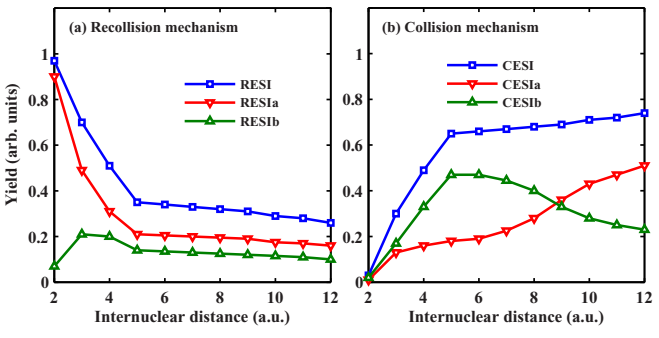

FIG. 5. (Color online) The CEP-averaged contributions of different ionization channels to the total DI yield for different internuclear distances.

Fig. 5(b), the contribution of the CESI channel increases quickly at first and then increases slowly as the internuclear distance increases. These results indicate that for small internuclear distances, the RESI channel is the dominant channel for DI, while for large internuclear distances, the CESI channel is predominantly responsible for the DI process. For moderate internuclear distances, both RESI and CESI channels contribute significantly to NSDI.

For the RESI and CESI channels, the two electrons are ionized one by one from the DES. Based on the ionization time, to discuss the transitions of different channels in detail, we further classify the DI process. If the two excited electrons are both released before the first maximum of the laser field after collision, the corresponding DI processes are identified as RESIa and CESIa, respectively. If only one excited electron is ionized before the first maximum of the laser field after collision and the other is released near the subsequent field maximum, the corresponding DI processes are identified as RESIb and CESIb, respectively. According to classical considerations [9], the two electrons from NSDI are more likely to be emitted into the same hemisphere when the DI events occur through the RESIa and CESIa channels, while, for the RESIb and CESIb channels, the electron pairs mainly escape into opposite hemispheres.

When $R = 2$ a.u., the statistical result reveals that nearly 90% of the DI events occur through the RESIa channel. This suggests that the correlated electron pairs are more likely to be emitted into the same hemisphere. Thus the CEP-averaged doubly-charged-ion momentum distributions exhibit a clear double-hump structure for the small internuclear distances [see Figs. 1(b) and 1(d)]. Comparing Fig. 1(b) with 1(d), one can see that the valley of the ion momentum distributions becomes shallow as the internuclear distance increases. This mainly originates from a decrease of the contribution of RESIa and increase of the contribution of CESIb to DI.

For $R = 5$ a.u., the sum of contributions of the RESIb and CESIb channels to the total DI yield is above 70%, which implies that the two electrons are emitted predominantly to opposite directions [9]. As a consequence, the CEP-averaged ion momentum distributions exhibit a single-hump structure [see Fig. 1(h)] and the amplitude of the asymmetry curve is very small [see Fig. 2(d)]. Note that for the CESIa channel, its contribution to the total DI increases slowly at first and then increases quickly as the internuclear distance increases [see Fig. 5(b)]. When $R = 12$ a.u., about 51% of the DI occurs through the CESIa channel, indicating that the CESIa channel plays an important role in NSDI at large internuclear distances. Furthermore, the statistical results show that the sum of contributions of the RESIb and CESIb channels is about 40%. Thus, the CEP-averaged ion momentum distributions exhibit a triple-hump structure for large internuclear distances [see Fig. 1(l)]. From the above discussion, we may draw the conclusion that with increasing internuclear distance, the process responsible for NSDI changes from the RESI channel to the CESI channel where the first electron ionizes along the internuclear axis, moves directly towards the other nucleus, and kicks out the second electron. This change leads to the result that the shape of the CEP-averaged ion momentum spectrum shows a double-single-triple peak structure as the internuclear distance increases.

V. THE CEP EFFECTS ON THE IONIZATION DYNAMICS

To explain the CEP-dependent asymmetry in the ions' momentum spectra, similarly to the previous studies for atoms [15,28], we discuss the CEP effects on the ionization dynamics of the first electron. The counts of DI events versus single-ionization time t_{i1} for internuclear distances $R = 2$ (the left column), 4 (the middle column), and 12 a.u. (the right column) are plotted in Fig. 6 for the CEP $\phi = 0$ (the top row), $\pi/6$ (the middle row), and $\pi/2$ (the bottom row). From Fig. 6, it is clearly seen that the distribution of the single-ionization times for $R = 2$ a.u. shows two peaks separated by the neighboring half cycle of the laser field [see Figs. 6(a)–6(c)]. However, for $R = 4$ and 12 a.u., the distributions exhibit a series of peaks [see Figs. 6(d)–6(i)]. In particular, Fig. 6 shows that as the CEP increases, not only the location but also the size of the peak is changed with a shift of the electric field peak.

The electric field of the laser pulse is plotted in Fig. 7, where the CEP is 0 and $\pi/6$. When the molecule is placed in such a pulse field, it can be ionized when the electric field is near the local maximum (or minimum). Under the present situation, the statistical results show that for the total DI events, more than 98% of the single-ionization processes occur during the four half cycles, as indicated by G_1, G_2, G_3, and G_4 in Fig. 7. The contributions of the four half cycles to the total DI yield are marked g_1, g_2, g_3, and g_4, respectively. Thus, in the following, we will analyze the CEP-dependent asymmetry in the ions' momentum spectra by considering the individual contributions from these four half cycles for different internuclear distances.

For $R = 2$ a.u., as shown in Figs. 6(a)–6(c), the single-ionization time is concentrated in two half cycles G_2 and G_3. Back analysis reveals that the negative ion momentum (see Fig. 1) is mainly due to the contribution of the half cycle G_2, and the positive ion momentum is mainly due to G_3. As a result, the asymmetry parameter is $(g_2 - g_3)$ for each CEP. With increase of the internuclear distance, because of the low ionization potential [25], the single-ionization processes occur during the four half cycles G_1, G_2, G_3, and G_4 [see Figs. 6(d)–6(i)]. The statistical results reveal that for $R = 4$, the contribution of half cycles G_2 and G_4 is responsible

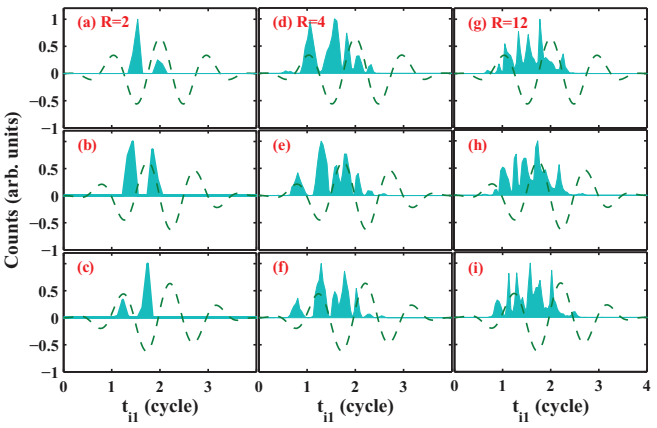

FIG. 6. (Color online) Counts of DI events versus single-ionization time t_{i1} for $R = 2$ (left column), 4 (middle column), and 12 a.u. (right column). The CEP $\phi = 0$ (top row), $\pi/6$ (middle row), and $\pi/2$ (bottom row).

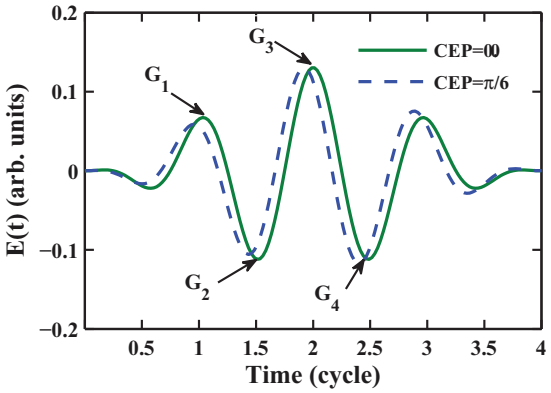

FIG. 7. (Color online) The electric field of a few-cycle pulse with $\phi = 0$ (solid line) and $\pi/6$ (dotted line). Four half cycles are denoted by G_1, G_2, G_3, and G_4. They move to the left as ϕ increases.

for the negative ion momenta and the positive ion momenta mainly originate from the contribution of G_1 and G_3. For $R = 12$ a.u., with the help of classical trajectory diagnosis, it is found that the CEP dependence of the asymmetric ion momentum distribution is mainly due to the contribution of the half cycles G_1, G_3, and G_4. The positive ion momenta derive from the contributions of G_1 and G_4 and the contribution of G_3 is responsible for the negative ion momenta. Although the contribution of G_2 to the total NSDI yield is about 50%, it has almost no effect on the asymmetry in the momentum distribution because it is uniformly distributed in the four quadrants for the two electrons from NSDI. As a consequence, the asymmetry parameters are $(g_2 + g_4) - (g_1 + g_3)$ and $g_3 - (g_1 + g_4)$ for $R = 4$ and 12 a.u., respectively.

As shown in Fig. 8, the CEP-resolved yields of the negative (dark blue filled circles and solid curves) and positive (purple empty circles and dotted curves) doubly-charged-ion momenta and the difference between the two yields (red empty circles and solid curves) for CEPs ranging from 0 to π are plotted for $R = 2,4,12$ a.u., respectively. Comparing with the Figs. 2(a), 2(c), and 2(f), the CEP-dependent asymmetry is well consistent for different internuclear distances. Therefore, the effects of CEP on the ionization dynamics of the first electron in the above-mentioned four half cycles dramatically affects the asymmetry in momentum, which depends sensitively on the internuclear distance.

An interesting result should be noted: for the total DI events, the distributions of the single ionization time for moderate and large internuclear distances show two peaks in a certain half cycle, as shown in Fig. 6 (see the middle and right columns). This behavior [multiple-ionization bursts (MIBs)] is first observed by solving the time-dependent Schrödinger equation and it is interpreted as transient electron location at one of the protons on the attosecond time scale [29]. By tracing the classical trajectories, it is found that for the RESI channels, the single ionizations often occur just after the peak of the electric field. Instead, for the CESI channels, the results show that almost all single ionizations occur just before the electric field maximum. Furthermore, back analysis reveals that the RESI channel is predominantly responsible for the NSDI process at small internuclear distances. Then the distribution of the single-ionization time exhibits a single-peak structure in a half cycle of the laser field (see the left column of Fig. 6), while for large internuclear distance, besides the RESI channel, the CESI channel plays an important role in NSDI, which means that for the total DI events, the distribution of the single-ionization time shows a double-peak structure in a half cycle of the laser field (see the right column of Fig. 6). As a result, the MIBs occur at large internuclear distance, but not at small internuclear distance.

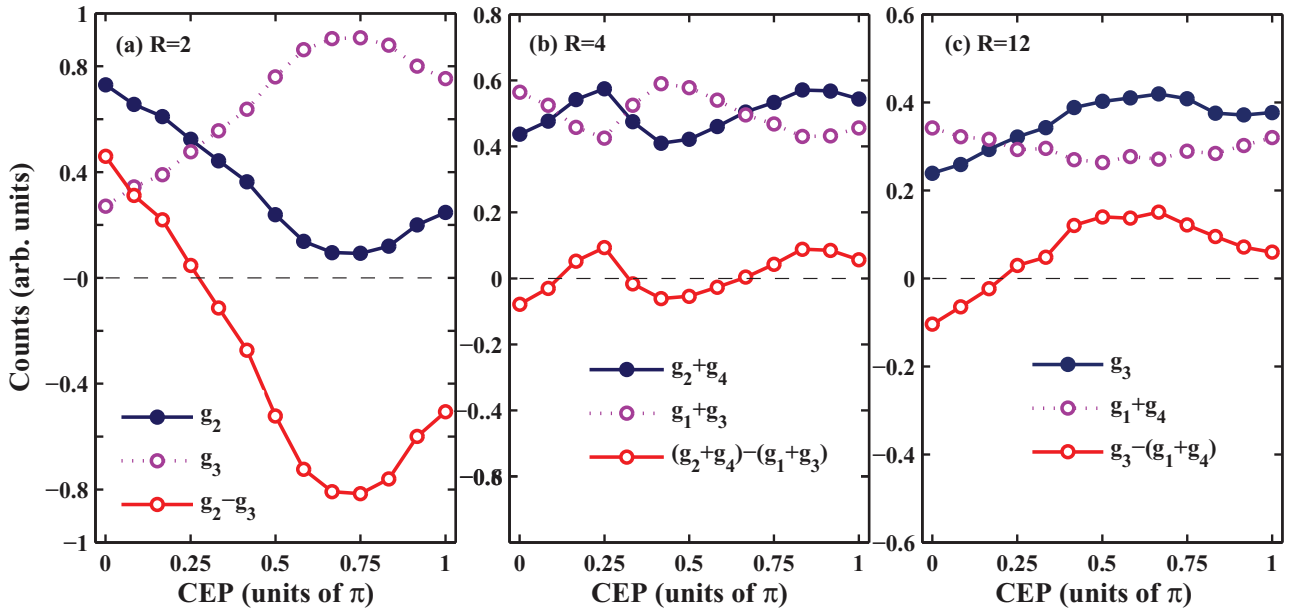

FIG. 8. (Color online) The CEP-resolved yields of the negative (dark blue filled circles and solid curves) and positive (purple empty circles and dotted curves) doubly charged ion momenta and the difference between the two yields (red empty circles and solid curves) for CEP ranging from 0 to π. $R = 2$ (a), 4 (b), and 12 a.u. (c), respectively.

VI. SUMMARY

In summary, the CEP dependence of the ionization dynamics in molecular NSDI driven by few-cycle laser pulses is investigated for different internuclear distances. The results show that the CEP-dependent asymmetry of the ion momentum spectra are different at different internuclear distances. By tracing the classical trajectories, it is found that the asymmetric ion momentum spectra are closely related to the ionization dynamics of the first electron. Back analysis reveals that with increase of the internuclear distance, the responsible DI mechanism transforms from the RESI channel to the CESI channel. This transformation of NSDI channels leads to the result that the shape of the CEP-averaged ion momentum spectrum shows a double-single-triple peak structure as the internuclear distance increases. These results represent an important step towards understanding the nature of the correlated dynamics of molecular DI with extended internuclear distances where the contribution of the CESI channel to NSDI can compete with that of the RESI channel.

ACKNOWLEDGMENTS

This work was supported by the National Natural Science Foundation of China under Grants No. 11234004, No. 61275126, and No. 11304265, the 973 Program of China under Grant No. 2011CB808103, and the Scientific Research Foundation of the Education Department of Henan Province in China under Grants No. 2011B140018 and No. 13A140774. Numerical simulations presented in this paper were carried out using the High Performance Computing Center experimental testbed in SCTS/CGCL (see http://grid.hust.edu.cn/hpcc).

[1] Th. Weber, H. Giessen, M. Weckenbrock, G. Urbasch, A. Staudte, L. Spielberger, O. Jagutzki, V. Mergel, M. Vollmer, and R. Dörner, Nature (London) **405**, 658 (2000); D. N. Fittinghoff, P. R. Bolton, B. Chang, and K. C. Kulander, Phys. Rev. Lett. **69**, 2642 (1992).

[2] B. Walker, B. Sheehy, L. F. DiMauro, P. Agostini, K. J. Schafer, and K. C. Kulander, Phys. Rev. Lett. **73**, 1227 (1994); Y. Zhou, Q. Liao, and P. Lu, Phys. Rev. A **80**, 023412 (2009).

[3] B. Feuerstein, R. Moshammer, D. Fischer, A. Dorn, C. D. Schröter, J. Deipenwisch, J. R. Crespo Lopez-Urrutia, C. Höhr, P. Neumayer, J. Ullrich, H. Rottke, C. Trump, M. Wittmann, G. Korn, and W. Sandner, Phys. Rev. Lett. **87**, 043003 (2001).

[4] A. Emmamouilidou, J. S. Parker, L. R. Moore, and K. T. Taylor, New J. Phys. **13**, 043001 (2011); Q. Liao, Y. Zhou, C. Huang, and P. Lu, *ibid.* **14**, 013001 (2012); M. Weckenbrock, D. Zeidler, A. Staudte, Th. Weber, M. Schöffler, M. Meckel, S. Kammer, M. Smolarski, O. Jagutzki, V. R. Bhardwaj, D. M. Rayner, D. M. Villeneuve, P. B. Corkum, and R. Dörner, Phys. Rev. Lett. **92**, 213002 (2004); C. Huang, Y. Zhou, A. H. Tong, Q. Liao, W. Hong, and P. Lu, Opt. Express **19**, 5627 (2011).

[5] A. Rudenko, K. Zrost, B. Feuerstein, V. L. B. de Jesus, C. D. Schröter, R. Moshammer, and J. Ullrich, Phys. Rev. Lett. **93**, 253001 (2004); Y. Zhou, C. Huang, Q. Liao, and P. Lu, *ibid.* **109**, 053004 (2012); A. Staudte, C. Ruiz, M. Schöffler, S. Schössler, D. Zeidler, Th. Weber, M. Meckel, D. M. Villeneuve, P. B. Corkum, A. Becker, and R. Dörner, *ibid.* **99**, 263002 (2007).

[6] X. Wang, J. Tian, and J. H. Eberly, Phys. Rev. Lett. **110**, 073001 (2013); C. Huang, Y. Zhou, Q. Zhang, and P. Lu, Opt. Express **21**, 11382 (2013); R. Kopold, W. Becker, H. Rottke, and W. Sandner, Phys. Rev. Lett. **85**, 3781 (2000).

[7] A. Becker, R. Dörner, and R. Moshammer, J. Phys. B: At. Mol. Opt. Phys. **38**, S753 (2005); Q. Liao and P. Lu, Phys. Rev. A **82**, 021403(R) (2010).

[8] M. Lein, E. K. U. Gross, and V. Engel, Phys. Rev. Lett. **85**, 4707 (2000); Y. Zhou, Q. Liao, and P. Lu, Phys. Rev. A **82**, 053402 (2010); Y. Zhou, C. Huang, A. H. Tong, Q. Liao, and P. Lu, Opt. Express **19**, 2301 (2011).

[9] P. B. Corkum, Phys. Rev. Lett. **71**, 1994 (1993); K. J. Schafer, B. Yang, L. F. DiMauro, and K. C. Kulander, *ibid.* **70**, 1599 (1993).

[10] T. Brabec and F. Krausz, Rev. Mod. Phys. **72**, 545 (2000); P. Lan, P. Lu, W. Cao, Y. Li, and X. Wang, Phys. Rev. A **76**, 011402(R) (2007); A. Baltuska, Th. Udem, M. Uiberacker, M. Hentschel, E. Goulielmakis, Ch. Gohle, R. Holzwarth, V. S. Yakovlev, A. Scrinzi, T. W. Hänsch, and F. Krausz, Nature (London) **421**, 611 (2003); J. Luo, Y. Li, Z. Wang, Q. Zhang, and P. Lu, J. Phys. B **46**, 145602 (2013).

[11] S. Zherebtsov, T. Fennel, J. Plenge, E. Antonsson, I. Znakovskaya, A. Wirth, O. Herrwerth, F. Süßann, C. Peltz, I. Ahmad, S. A. Trushin, V. Pervak, S. Karsch, M. J. J. Vrakking, B. Langer, C. Graf, M. I. Stockman, F. Krausz, E. Rühl, and M. F. Kling, Nat. Phys. **7**, 656 (2011); B. Bergues, S. Zherebtsov, Y. Deng, X. Gu, I. Znakovskaya, R. Kienberger, F. Krausz, G. Marcus, and M. F. Kling, New J. Phys. **13**, 063010 (2011); P. Lan, P. Lu, W. Cao, and X. Wang, J. Phys. B **40**, 403 (2007).

[12] G. G. Paulus, F. Grasbon, H. Walther, P. Villoresi, M. Nisoli, S. Stagira, E. Prior, and D. Silvestri, Nature (London) **414**, 182 (2001).

[13] X. Liu and C. Figueira de Morisson Faria, Phys. Rev. Lett. **92**, 133006 (2004); H. Rottke, X. Liu, E. Ermina, M. Sandner, E. Goulielmakis, K. O. Keeffe, M. Lezius, F. Krausz, F. Lindner, M. G. Schätzel, G. G. Paulus, and H. Walther, J. Mod. Opt. **53**, 149 (2006).

[14] M. F. Kling, C. Siedschlag, A. J. Verhoef, J. I. Khan, M. Schultze, T. Uphues, Y. Ni, M. Uiberacker, M. Drescher, F. Krausz, and M. J. J. Vrakking, Science **312**, 246 (2006); P. Lan, E. J. Takahashi, K. Liu, Y. Fu, and K. Midorikawa, New J. Phys. **15**, 063023 (2013); P. Lan, E. J. Takahashi, and K. Midorikawa, Phys. Rev. A **86**, 013418 (2012); K. Liu, W. Hong, Q. Zhang, and P. Lu, Opt. Express **19**, 26359 (2011).

[15] C. F. Faria, X. Liu, A. Sanpera, and M. Lewenstein, Phys. Rev. A **70**, 043406 (2004); Q. Liao, P. Lu, Q. Zhang, W. Hong, and Z. Yang, J. Phys. B **41**, 125601 (2008); S. Micheau, Z. Chen, A. T. Le, and C. D. Lin, Phys. Rev. A **79**, 013417 (2009).

[16] N. Camus, B. Fischer, M. Kremer, V. Sharma, A. Rudenko, B. Bergues, M. Kübel, N. G. Johnson, M. F. Kling, T. Pfeifer, J. Ullrich, and R. Moshammer, Phys. Rev. Lett. **108**, 073003 (2012).

[17] B. Bergues, M. Kübel, N. G. Johnson, B. Fischer, N. Camus, K. J. Betsch, O. Herrwerth, A. Senftleben, A. M. Sayler, T. Rathje, I. Ben-Itzhak, R. R. Jones, G. G. Paulus, F. Krausz, R. Moshammer, J. Ullrich, and M. F. Kling, Nat. Commun. **3**, 813 (2012).

[18] M. Kübel, Nora G. Kling, K. J. Betsch, N. Camus, A. Kaldun, U. Kleineberg, I. Ben-Itzhak, R. R. Jones, G. G. Paulus, T. Pfeifer, J. Ullrich, R. Moshammer, M. F. Kling, and B. Bergues, Phys. Rev. A **88**, 023418 (2013).

[19] C. Cornaggia and Ph. Hering, Phys. Rev. A **62**, 023403 (2000).

[20] H. Yu, T. Zuo, and A. D. Bandrauk, Phys. Rev. A **54**, 3290 (1996); T. Zuo and A. D. Bandrauk, *ibid.* **52**, R2511 (1995); S. Saugout, E. Charron, and C. Cornaggia, *ibid.* **77**, 023404 (2008).

[21] T. Havermeier, T. Jahnke, K. Kreidi, R. Wallauer, S. Voss, M. Schöffler, S. Schössler, L. Foucar, N. Neumann, J. Titze, H. Sann, M. Kühnel, J. Voigtsberger, A. Malakzadeh, N. Sisourat, W. Schollkopf, H. Schmidt-Bocking, R. E. Grisenti, and R. Dörner, Phys. Rev. Lett. **104**, 153401 (2010).

[22] H. Ni, C. Ruiz, R. Dörner, and A. Becker, Phys. Rev. A **88**, 013407 (2013).

[23] P. J. Ho, R. Panfili, S. L. Haan, and J. H. Eberly, Phys. Rev. Lett. **94**, 093002 (2005); S. L. Haan, L. Breen, A. Karim, and J. H. Eberly, *ibid.* **97**, 103008 (2006).

[24] S. L. Haan, J. S. Van Dyke, and Z. S. Smith, Phys. Rev. Lett. **101**, 113001 (2008); S. L. Haan, Z. S. Smith, K. N. Shomsky, and P. W. Plantinga, J. Phys. B **42**, 134009 (2009); Y. Zhou, Q. Liao, Q. Zhang, W. Hong, and P. Lu, Opt. Express **18**, 632 (2010).

[25] T. T. Nguyen-Dang, F. Châteauneuf, S. Manoli, O. Atabek, and A. Keller, Phys. Rev. A **56**, 2142 (1997).

[26] Y. Zhou and P. Lu, Front. Optoelectron. China **3**, 184 (2010); Q. Tang, Y. Zhou, C. Huang, Q. Liao, and P. Lu, Opt. Express **20**, 19580 (2012); Q. Tang, D. Zhang, M. Liu, Y. Gao, and B. Yu, Opt. Commun. **307**, 32 (2013).

[27] A. Tong, Y. Zhou, C. Huang, and P. Lu, J. Chem. Phys. **139**, 074308 (2013).

[28] C. F. Faria, T. Shaaran, and M. T. Nygren, Phys. Rev. A **86**, 053405 (2012).

[29] N. Takemoto and A. Becker, Phys. Rev. Lett. **105**, 203004 (2010).